INTERNATIONAL JOURNAL OF
COASTAL, OFFSHORE & ENVIRONMENTAL ENGINEERING
IJCOE Vol.11/No. 2/Spring 2026 (12-25)

Available online at: www. Ijcoe.org

Hydrodynamic Effects of Cap Water Entry on Subsea Distribution Unit Suction Caisson Foundation Lowering Response

Mehdi Shirani[1]

[1] *Assistant Professor, Research Institute for Subsea Science and Technology, Isfahan University of Technology, Isfahan, Iran; mehdi.shirani@iut.ac.ir*

ARTICLE INFO

Article History:
Received 18 oct 2025
Accepted 18 Feb 2025

Keywords:
Subsea Distribution Unit (SDU)
Suction caisson
Offshore lowering
Operability
OrcaFlex

ABSTRACT

Lowering a suction-caisson-type subsea structure through the splash zone is a difficult modelling problem because the governing response is controlled by rapidly changing hydrodynamic conditions at free-surface crossing. This paper presents a time-domain OrcaFlex analysis of the lifting and lowering of a Subsea Distribution Unit (SDU) Suction Caisson foundation. The hydrodynamic representation combines a main hollow-body spar-buoy model with two auxiliary buoy corrections: one to account for the additional axial added mass that develops when the caisson cap crosses the free surface, and one to account for the inertia of the water entrapped within the structure after submergence. Environmental screening was performed in the time domain using deterministic regular waves over a matrix of wave heights, periods, and headings. The operability maps show that the splash-zone stage governs the operation. A dedicated case study for wave direction 0°, H = 0.5 m, and T = 6 s further demonstrates the sensitivity of the response to the auxiliary buoy modelling. Relative to the base model without the two auxiliary buoys, activating the entrapped-water buoy increases the peak crane-cable tension from about 680 kN to 779 kN, while activating both the entrapped-water and axial-added-mass buoys raises it to about 907 kN and produces the longest post-entry oscillations. The results confirm that realistic suction-caisson lowering analysis requires explicit treatment of both entrapped-water inertia and cap-entry axial added mass, because these mechanisms control the transient splash-zone response and the resulting operability limits.

1. Introduction

Subsea suction caisson installation is one of the most hydrodynamically sensitive operations in offshore oil and gas field development because the governing response often occurs during sea-surface crossing, when the structure transitions from an in-air body to a partially submerged, then fully submerged, body within a short time window [1-5]. In this stage, the payload is influenced simultaneously by vessel-motion transfer through the crane system, time-varying buoyancy, drag, free-surface effects, rapidly increasing added mass, and, for partially enclosed geometries, the inertia of water that becomes trapped inside the structure [1,2,4,5]. As a result, splash-zone lowering of suction-caisson-type bodies cannot be reliably assessed using a simplified, fully submerged representation alone [2,4,5].

In offshore oil and gas developments, a Subsea Distribution Unit (SDU) is a subsea-installed unit that supports the distribution and connection of production, control, and utility functions within the subsea system [6]. Depending on the field architecture, the unit may form part of a foundation-supported subsea arrangement that connects or supports associated subsea hardware on the seabed [6]. In the present study, the analysed SDU suction caisson foundation is treated as a foundation-supported subsea distribution unit with suction-caisson-type characteristics. From an installation perspective, it functions as a tall, partially enclosed tubular body with a capped upper region and an internal cavity. These geometric features are crucial because they govern the hydrodynamic response during free-surface crossing and directly affect crane-cable tension, declination, and operability.

A substantial portion of the published literature on subsea installation has focused on splash-zone phenomena, as this stage is often associated with the most severe transient hydrodynamic response [1-5]. Review of work on subsea lifting modelling has shown that splash-zone crossing, the fully submerged stage, and the near-seabed stage are the main response windows of interest, while free-surface loading, transient hydrodynamics, and operability assessment remain challenging topics [1]. Studies on subsea templates, spool pieces, subsea trees, and other lowered structures have similarly shown that time-domain modelling is required when allowable sea states are governed by transient coupled response rather than by a single quasi-static load measure [2-4].

For suction-caisson-type structures, however, the modelling challenge is even more specific. When the caisson cap approaches and then hits the water surface, the body no longer behaves as a simple hollow tubular frame. Instead, the free-surface intersection can generate a rapid increase in axial added mass, while continued submergence may produce the inertia of water entrapped inside the caisson [5]. These mechanisms alter the vertical hydrodynamic inertia, influence the stability of structural motion, and can produce pronounced fluctuations in crane-cable motion during lowering [5]. Previous studies on suction-pile or suction-anchor lowering have highlighted the importance of proper splash-zone modelling, but there remains a practical need for engineering studies that translate these hydrodynamic effects into response-based operability criteria directly useful for offshore execution [5].

The present paper addresses this need by analysing the lifting and lowering of an SDU foundation using a staged time-domain OrcaFlex model. Particular attention is given to the hydrodynamic idealisation required to represent suction-caisson behaviour at sea-surface crossing [5]. The SDU foundation is modelled using a main hollow-body buoy representation supplemented by two local auxiliary buoy corrections: one for the additional axial added mass that develops when the upper cap crosses the free surface, and one for the inertia of the water entrapped inside the structure after cap submergence [5]. The main purpose of the paper is therefore not only to assess operability, but also to show why realistic suction-caisson lowering analysis requires explicit treatment of cap-entry hydrodynamics [5].

The objective of the study is to determine the governing installation stage of the SDU foundation and to quantify the influence of splash-zone hydrodynamics on crane-cable response. The novelty of the work lies in three main aspects. First, it focuses specifically on the lowering behaviour of a suction-caisson-type subsea foundation structure rather than on an open-frame subsea unit. Second, it develops a practical OrcaFlex [7] modelling strategy to represent both entrapped-water inertia and the additional axial added mass arising when the suction caisson cap intersects the free surface. Third, it demonstrates that the governing operability stage is the splash zone, where cap-water interaction destabilises the lowering response and increases crane-cable fluctuations, rather than the fully submerged lowering phase. The study is therefore intended to provide both a project-relevant assessment and a more general modelling framework for suction-caisson splash-zone analysis.

2. Description of the installation system

Figure 1 presents the analysed SDU foundation geometry together with the equivalent OrcaFlex idealisation used in the numerical model. Figure 1(a) shows an isometric view of the analysed SDU foundation, while Figure 1(b) shows the equivalent OrcaFlex model. In Figure 1(b), the auxiliary buoy “AxialAddedMassTopSeaSurface” is indicated in blue, and the auxiliary buoy “ExtraMassTrappedWater” is indicated in red.

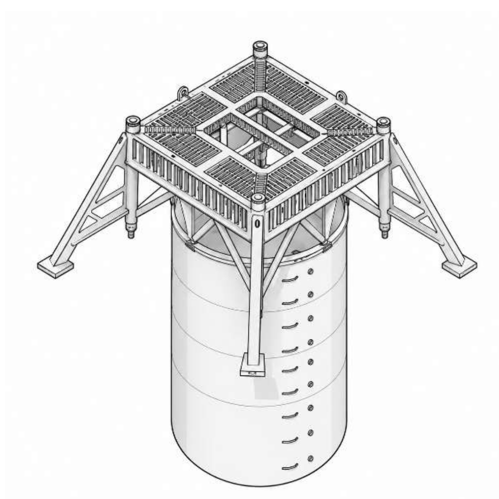

(a)

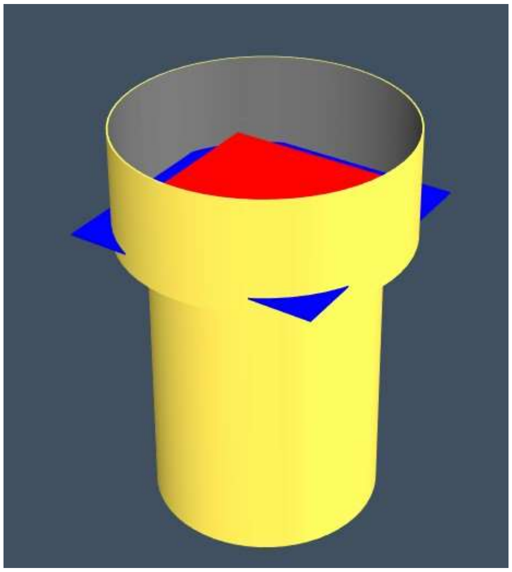

(b)

Figure 1- (a) Isometric view of the analysed SDU foundation; (b) equivalent OrcaFlex model, the auxiliary buoy "AxialAddedMassTopSeaSurface" is shown in blue, and the auxiliary buoy "ExtraMassTrappedWater" is shown in red.

The main properties adopted for the numerical model are summarised in Table 1.

Table 1- Main properties of the SDU foundation used in the numerical model.

Property	Value
Width	7.0 m
Height	12.5 m
Dry installation weight in air	68.878 t
Fully submerged weight	59.218 t
Buoyancy during lowering	8.954 t
Displaced volume in seawater (ρ = 1.025 t/m³)	8.736 m³
Centre of gravity, x	0.0 m
Centre of gravity, y	0.0 m
Centre of gravity, z	7.9 m
Ixx about the centre of mass	1500 t·m²
Iyy about the centre of mass	1500 t·m²
Izz about the centre of mass	1119.3 t·m²

3. Numerical methodology
3.1 OrcaFlex model formulation

The dynamic installation model was developed in OrcaFlex v11.6b using the time-domain approach. The vessel motions were introduced through imported response amplitude operators (RAOs) derived from third-party diffraction analysis. During lift-off from the cargo barge, non-axisymmetric two-body RAOs for the installation vessel and the barge were used. During lowering after barge departure, single-body RAOs for the installation vessel were used and treated as axisymmetric for operability assessment.

Figure 2 shows the OrcaFlex model set-up adopted for the two principal installation stages. Figure 2(a) illustrates the lifting model, while Figure 2(b) shows the lowering model after barge departure.

(a)

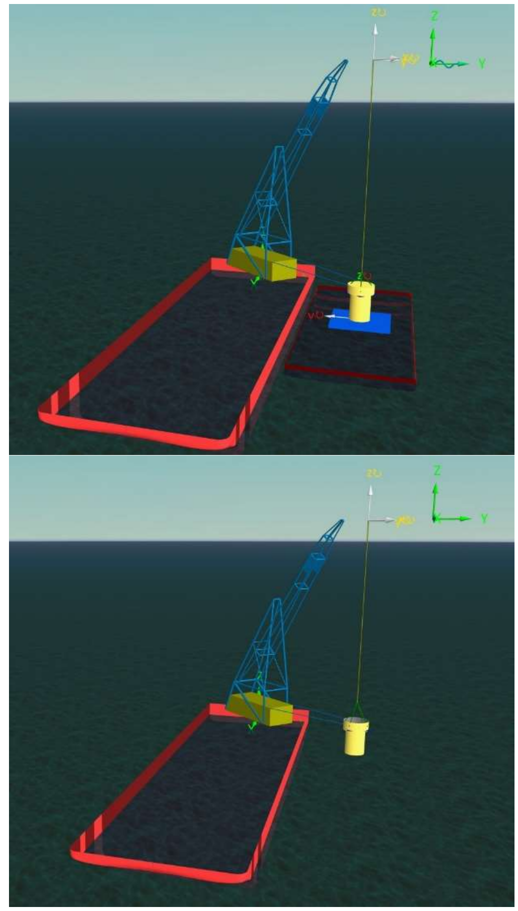

(b)

Figure 2- OrcaFlex model set-up for the analysed installation stages: (a) lifting model; (b) lowering model.

Figure 3 shows the axes directions and sign convention used in OrcaFlex for the vessel coordinate system.

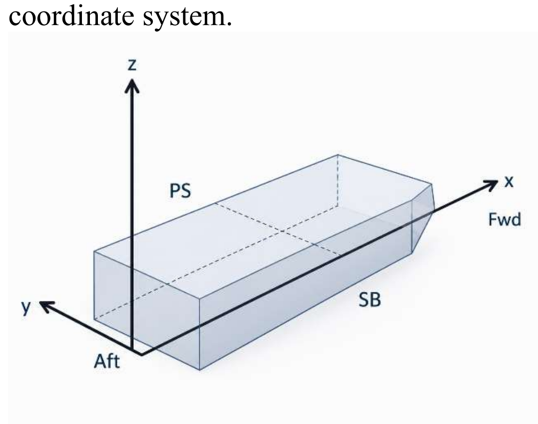

Figure 3- OrcaFlex axes in the vessel coordinate system.

3.2 Environmental conditions

The wave data used in the environmental screening are summarised in Table 2, which reports the wave height H, the associated wave period T, and the analysed wave directions. Figure 4 shows the wave angle relative to the vessel.

The environmental screening analyses were carried out in the time domain using deterministic regular waves defined by wave direction, height, and period. In the OrcaFlex model, the regular-wave kinematics were represented using Dean stream-function wave theory with stream-function order 5. The regular-wave cases were used as the primary design-wave simulations for operability screening.

Table 2. Wave data used in the environmental screening.

Parameter	Unit	Value
H	m	0.25–2.0 with step 0.25
T	s	4.0–14.0 with step 1
Wave direction	degree	0–360 with step 22.5

Figure 4 illustrates the wave directions defined relative to the vessel, which are used throughout the hydrodynamic and operability assessments.

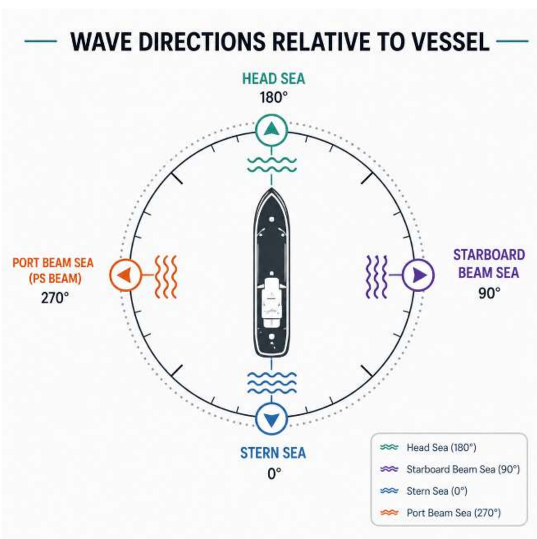

Figure 4- Wave directions relative to the vessel.

For the lift-off phase, where the installation vessel and cargo barge were modelled together, the motion input was based on the corresponding two-body RAOs. Because these RAOs are non-axisymmetric, operability for this phase was assessed for wave headings from 0° to 337.5° in 22.5° increments, giving 16 analysed directions. Combined with 8 wave-height cases and 11 wave-period cases, this produced a total of 1408 regular-wave load cases for the lift-off model.

For the lowering model, after the barge had departed, only the installation vessel remained in the simulation, and the motion input was based on single-body RAOs treated as axisymmetric. Accordingly, the directional range was reduced to 0° to 180°, which corresponds to 9 analysed headings with the same 22.5° increment. Using the same H and T ranges, therefore, yielded 792 regular-wave load cases for the lowering model.

Water depth was 154 m, and seawater density was taken as 1025 kg/m³. Current and marine growth were neglected in the present analysis, consistent with the adopted modelling basis.

3.3 Hydrodynamic coefficients

The adopted hydrodynamic values are summarised in Table 3. The added-mass coefficient taken from DNV guidance [8-9] was converted to the corresponding OrcaFlex Ca format.

Table 3- Calculated hydrodynamic coefficients adopted for the SDU foundation suction caisson model.

Geometry	Added Mass Normal	Added Mass Axial	Drag Normal	Drag Axial	Slamming coeff.	Reference
Tubular structures	1.0	N.A.	0.85	0.008	N.A.	DNV-RP-C205 [8] / DNV-RP-N103 [9]

3.4 Hydrodynamic representation of the SDU foundation

The hydrodynamic model of the SDU foundation was implemented using one main 6D spar buoy and two auxiliary 6D lumped buoys, Figure 2(b). The main spar buoy, denoted “SDU-FOUNDATION”, represents the principal tubular geometry of the SDU foundation and carries the global structural mass, centre of gravity, rigid-body inertia, buoyancy variation, and the general drag response of the foundation during lifting, splash-zone crossing, and lowering.

For most of the splash-zone lowering operation, water inside the suction caisson can move axially in and out through the bottom opening, so the axial added-mass effect remains limited. However, once the top cap approaches and contacts the water surface, the water inside the caisson can no longer move freely. Instead, part of the internal water becomes constrained to move together with the structure in the vertical direction. As a result, both the effective axial added mass and the associated fluid inertia increase during free-surface crossing.

In addition to this increase in outer-body axial added mass, a further hydrodynamic effect develops after cap submergence: an internal body

of water becomes entrapped within the caisson cavity, contributing additional vertical inertia to the lowering system. To represent these mechanisms in OrcaFlex, the SDU foundation model was divided into three buoy objects: one spar buoy carrying the main physical and hydrodynamic properties of the structure, one lumped buoy representing the additional axial added mass that develops when the cap hits the sea surface, and one lumped buoy representing the entrapped water inside the suction caisson.
The conceptual arrangement of the three buoy objects used to represent the main suction caisson, the additional axial added mass, and the entrapped water is shown in Figure 5.

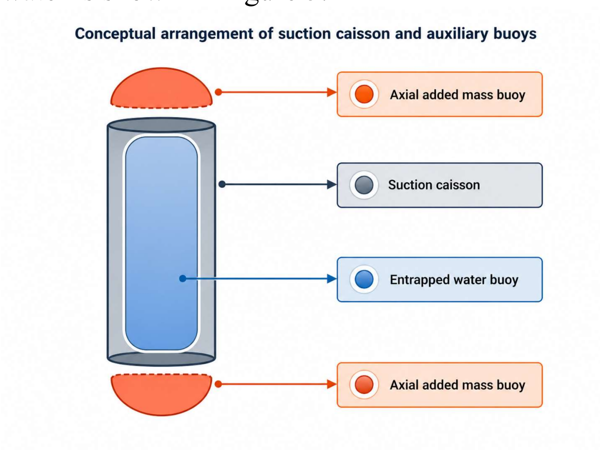

Figure 5- Conceptual sketch of the suction caisson model showing the auxiliary buoy arrangement used to represent axial added mass and entrapped water.

3.4.1 Additional axial added mass at sea-surface crossing

The purpose of this calculation is to estimate the additional vertical hydrodynamic inertia that develops when the top cap of the suction caisson crosses the water surface. At this stage, the structure no longer behaves like a simple slender body moving in open water. Instead, the presence of the cap and the vertical-sided caisson geometry cause the surrounding water to resist the vertical motion more strongly. In practical terms, this manifests as an increase in heave added mass, which must be included in the OrcaFlex model to realistically reproduce the splash-zone response.

For the analysed SDU suction caisson, the main geometric parameters are:

- Outer diameter, $OD = 7.0$ m
- Inner diameter, $ID = 6.96$ m
- Suction caisson height, $h = 9.5$ m

The seawater density is taken as:

$$\rho = 1025\ \text{kg/m}^3$$

Following the simplified DNV-RP-N103 [9] method for three-dimensional bodies with vertical sides, the first step is to evaluate the vertical-sides parameter:

$$\lambda = \frac{\sqrt{A_P}}{h + \sqrt{A_P}}$$

where A_P is the horizontal projected area of the caisson. For the present circular outer geometry,

$$A_P = \frac{\pi OD^2}{4} = \frac{\pi (7.00)^2}{4} = 38.4845\ \text{m}^2$$

and therefore

$$\sqrt{A_P} = 6.2036\ \text{m}$$

Substituting into the definition of λ,

$$\lambda = \frac{6.2036}{9.50 + 6.2036} = 0.3950$$

The parameter λ expresses the relative importance of the caisson plan area compared with its height and is used in the DNV method [9] to correct the heave added mass for a three-dimensional body with vertical sides.

The corresponding DNV [9] height-correction expression is:

$$A_{33} = \left[1 + \sqrt{\frac{1-\lambda^2}{2(1+\lambda^2)}}\right] A_{33o}$$

where:

- A_{33} is the corrected heave added mass of the outer body,
- A_{33} is the reference heave added mass for a flat circular disc.

Substituting $\lambda = 0.3950$,

$$\frac{A_{33}}{A_{33o}} = 1 + \sqrt{\frac{1 - 0.3950^2}{2(1 + 0.3950^2)}} = 1.6042$$

Hence,

$$A_{33.\text{outer}} = 1{,}6042\, A_{33o}$$

The reference added mass A_{33} is taken from the flat-disc expression in the DNV guidance [9]. Using the outer radius of the caisson,

$$a = \frac{OD}{2} = 3.50 \text{ m}$$

the reference disc added mass becomes:

$$A_{33o} = \frac{8}{3}\rho a^3$$

Thus,

$$A_{33} = \frac{8}{3}(1025)(3.50)^3 = 117{,}193 \text{ kg}$$

or

$$A_{33o} \approx 117.2 \text{ t}$$

Therefore, the corrected outer-body heave added mass is:

$$A_{33,\text{outer}} = 1.6042 \times 117{,}193 = 188{,}064 \text{ kg}$$

that is,

$$A_{33,\text{outer}} \approx 188.1 \text{ t}$$

This value represents the additional vertical added mass associated with the outer caisson body when the cap region interacts with the free surface. In the present modelling approach, this added mass is assigned to the auxiliary buoy "AxialAddedMassTopSeaSurface" in OrcaFlex.

Following the Orcina *F07 Suction Anchor Lowering* [10] modelling approach, the buoy is specified using:

- Hydrodynamic mass in Z: 188.1 t
- $C_a(z) = 1.0$

At this point, it is useful to clarify why both hydrodynamic mass and an inertia coefficient are specified. In OrcaFlex, the axial added-mass behaviour can be represented in terms of a coefficient relative to the displaced mass of the buoy. Since the hydrodynamic mass has already been determined from the DNV formula [9], the corresponding displaced-water-based inertia coefficient must be back-calculated so that the OrcaFlex buoy reproduces the same effective axial inertia.

This is done from:

$$C_m = 1 + \frac{\Delta}{A_{33,\text{outer}}}$$

where Δ is the displaced mass of water associated with the outer caisson volume:

$$\Delta = \rho A_P h$$

Substituting the present dimensions,

$$\Delta = 1025 \times \frac{\pi(7.00)^2}{4} \times 9.50 = 374{,}805 \text{ kg}$$

Hence,

$$C_m = 1 + \frac{374{,}805}{188{,}064} = 2.99$$

Therefore, for the buoy "AxialAddedMassTopSeaSurface",

$$C_m(z) \approx 2.99$$

In physical terms, this means that the buoy is calibrated so that its vertical dynamic response reproduces the solid-body-like axial added mass generated when the suction caisson cap crosses the sea surface. The procedure follows the Orcina modelling philosophy: first, determine the required axial hydrodynamic mass from theory; then, back-calculate the inertia coefficient so that the OrcaFlex buoy reproduces the same effective added-mass behaviour.

As a result, the buoy "AxialAddedMassTopSeaSurface" does not represent the global buoyancy of the whole SDU foundation. Instead, it is a local hydrodynamic correction introduced only to capture the extra axial inertia that becomes important during free-surface crossing.

3.4.2 Entrapped-water inertia after top-cap submergence

In addition to the outer-body axial added mass, a second hydrodynamic effect must be represented during lowering. Once the top cap of the suction caisson has passed below the water surface, water becomes trapped inside the caisson cavity and can no longer move freely as the structure continues to descend. This trapped internal water does not provide additional buoyancy in the usual sense, since the overall hydrostatic behaviour is already accounted for by the main SDU spar buoy. However, it does contribute inertia, since part of the internal water column is effectively forced to move together with the structure in the vertical direction.

For this reason, the trapped-water effect is represented separately in the OrcaFlex model by the auxiliary buoy "ExtraMassTrappedWater". The role of this buoy is not to represent geometry or hydrostatics, but only to add the correct vertical hydrodynamic mass associated with the internal water column after top-cap submergence.

The trapped-water volume is estimated from the internal cylindrical volume of the suction caisson:

$$V_{\text{trapped}} = \frac{\pi ID^2 h}{4}$$

where:

- $ID = 6.96$ mis the inner diameter of the suction caisson,
- $h = 9.5$ mis the caisson height,
- $\rho = 1025\ \text{kg/m}^3$is the seawater density.

Substituting the present dimensions,

$$V_{\text{trapped}} = \frac{\pi(6.96)^2(9.50)}{4} = 361.44\ \text{m}^3$$

The corresponding trapped-water mass is then:

$$M_{\text{trapped}} = \rho V_{\text{trapped}}$$

Hence,

$$M_{\text{trapped}} = 1025 \times 361.44 = 370{,}472\ \text{kg}$$

or, equivalently,

$$M_{\text{trapped}} \approx 370.5\ \text{t}$$

For modelling purposes, this value was rounded and entered in OrcaFlex as approximately:

$$M_{\text{trapped}} \approx 370\ \text{t}$$

in the vertical hydrodynamic mass term of the buoy "ExtraMassTrappedWater".

It is important to clarify the physical meaning of this modelling step. The buoy "ExtraMassTrappedWater" is introduced only to represent the inertial effect of the internal water column after submergence. It is not intended to introduce additional structural mass, additional hydrostatic volume, or additional drag loading. Those effects are already represented elsewhere in the model, primarily through the main spar buoy and the structural properties assigned to the SDU foundation.

For this reason, the buoy was configured to contribute only inertia. In practice, this was achieved by assigning:

- negligible geometric volume,
- hydrodynamic mass in Zequal to approximately 370 t,
- $C_a(z) = 1.0$,
- $C_m(z) = 0.0$,

while all remaining translational and rotational hydrodynamic coefficients were set to zero.

This choice ensures that the buoy does not create artificial buoyancy or drag forces. Instead, it acts purely as a lumped vertical inertia term that becomes active once the caisson top is submerged and the internal water is effectively carried with the structure.

From a physical point of view, this modelling assumption reflects the fact that the internal water column resists rapid changes in vertical motion. As a result, once the SDU enters the water and the upper cap passes below the free surface, the trapped water increases the system's effective vertical inertia. This can amplify the transient response during splash-zone crossing and influence both crane-cable tension and cable-angle behaviour.

3.4.3 Functional separation of the buoy objects

The use of three separate buoy objects in the OrcaFlex model is intentional and reflects that different parts of the SDU's hydrodynamic response are governed by distinct physical mechanisms.

The main spar buoy, denoted “SDU-FOUNDATION”, represents the global geometry and hydrostatic behaviour of the subsea structure. It carries the principal structural mass, centre of gravity, rigid-body inertia, buoyancy variation, and the general drag response of the SDU foundation during lifting, splash-zone crossing, and lowering. In other words, this buoy is the main hydrodynamic representation of the foundation structure as a whole.

However, the main spar buoy alone is not sufficient to reproduce the two localised hydrodynamic effects that become important when the suction caisson cap approaches and passes through the free surface: the additional axial added mass generated at sea-surface crossing, and the inertia of the water trapped inside the caisson after the top cap has submerged. For this reason, two auxiliary buoy objects were introduced.

The first auxiliary buoy, “AxialAddedMassTopSeaSurface”, represents the additional vertical added mass associated with free-surface crossing. Its purpose is to account for the increased resistance of the surrounding water to vertical motion when the upper cap of the caisson interacts with the sea surface. This buoy is therefore a local hydrodynamic correction for axial inertia and is not intended to represent the overall buoyancy of the structure.

The second auxiliary buoy, “ExtraMassTrappedWater”, represents the vertical inertia of the internal water column once the cap has submerged and water has become trapped in the caisson cavity. This buoy likewise acts only as an inertial correction and does not represent additional hydrostatic volume or additional structural weight.

This functional separation is important because it avoids double-counting. The main spar buoy already reproduces the SDU’s global displaced volume and hydrostatic response. If the auxiliary buoy objects were also allowed to contribute normal buoyancy in the same way, the model would artificially overestimate the hydrodynamic forces. By assigning the auxiliary buoys only the specific inertial functions required, the model preserves the correct global buoyancy while still capturing the local splash-zone physics.

Accordingly, the modelling roles of the three buoy objects may be summarised as follows: “SDU-FOUNDATION” represents the global structural and hydrostatic response of the SDU foundation; “AxialAddedMassTopSeaSurface” provides a local correction for the additional axial added mass at cap-entry/free-surface crossing; and “ExtraMassTrappedWater” provides a local correction for the inertia of the entrapped internal water after top-cap submergence. This modelling strategy provides a practical balance between physical realism and numerical simplicity. The overall SDU foundation response is governed by the main spar buoy, while the two auxiliary buoys are used only to introduce the specific splash-zone hydrodynamic effects that would otherwise be underrepresented.

3.5 Installation stages and model configuration

The analysed offshore operation was represented through two sequential numerical models. In the first model, the SDU foundation was positioned on the cargo barge and lifted by the installation vessel. Both the installation vessel and the barge were included in the numerical model because their relative motions directly influence crane-cable tension, clearance behaviour, and contact response. In the second model, the barge was removed, and the installation vessel continued lowering the SDU foundation from the suspended condition to the seabed.

In the lift-off model, the first 300 s of simulation time were used for wave build-up. The SDU foundation then remained seated on the barge for 600 s under fully developed environmental loading. Thereafter, it was lifted 3 m above the deck and held in the air for an additional 600 s. In the lowering model, the SDU foundation was first held in the air after barge departure, then the outreach was reduced, the structure was lowered into the water, the tugger lines were released, and the SDU foundation was lowered to the seabed.

For interpretation and post-processing, the overall operation was reported in three operational windows: (i) Lifting Off the Deck; (ii) Splash Zone, from the time the bottom of the SDU foundation was 1 m above the sea surface until the top of the structure was 1 m below the surface; and (iii) Lowering, from that point until seabed landing.

4 Acceptance criteria and post-processing

Operability was assessed using the following criteria: crane-cable DAF ≤ 2.0; absolute off-lead angle ≤ 2.0°, and absolute side-lead angle ≤ 2.0°. For each load case, the maximum response within the relevant time window was extracted and used to derive limiting sea-state tables and operability plots. Post-processing focused on crane-cable tension, DAF, off-lead angle, and side-lead angle for the Lifting Off the Deck, Splash Zone, and Lowering windows.

5 Results and discussion

5.1 Overall operability trends

The operability assessment shows a clear hierarchy among the three analysed installation stages. Figures 6–8 allow the limiting significant wave height to be compared directly as a function of wave direction and peak period for the three principal operational windows: Lifting Off the Deck, Splash Zone, and Lowering. The splash-zone phase governs the overall operation, the lift-off phase is a secondary but still sensitive stage, and the fully submerged lowering stage is less restrictive overall.

A consistent pattern is visible across Figures 6–8. For both lift-off and fully submerged lowering, the DAF-based envelopes are comparatively permissive and, in many regions, reach the upper screened limit of H = 2.0 m, whereas the off-lead and side-lead criteria impose the main restrictions. In the splash zone, by contrast, the weather window narrows because short-period cases are already limited by DAF, and a broad band of intermediate periods is further constrained by the lead-angle response. The governing weather window is therefore defined by the combined action of free-surface-entry hydrodynamics and crane-wire angular demand rather than by dynamic amplification alone.

5.2 Lifting off the deck

The lift-off-stage operability results are summarised in Figure 6. Figure 6(a) presents the crane-cable dynamic amplification factor (DAF), Figure 6(b) presents the absolute off-lead angle, and Figure 6(c) presents the absolute side-lead angle. The DAF plot is comparatively permissive: for most headings and periods, the limiting sea state remains in the range of about 1.5–2.0 m, and many cases reach the upper screened limit of 2.0 m. Only local reductions are observed, mainly around intermediate periods near 8–10 s.

The angle-based criteria are more restrictive. Figures 6(b) and 6(c) show that both off-lead and side-lead reduce the allowable H over several oblique headings, particularly around intermediate periods near 10–12 *s*, where some cases fall below 1.0 *m*, and isolated cells fail even at the minimum screened sea state. The off-lead response is slightly more restrictive than the side-lead response in several sectors, but both criteria are materially tighter than the DAF criterion. These results show that lift-off is operationally important and requires careful planning, yet it does not define the narrowest overall weather window for the analysed SDU foundation installation.

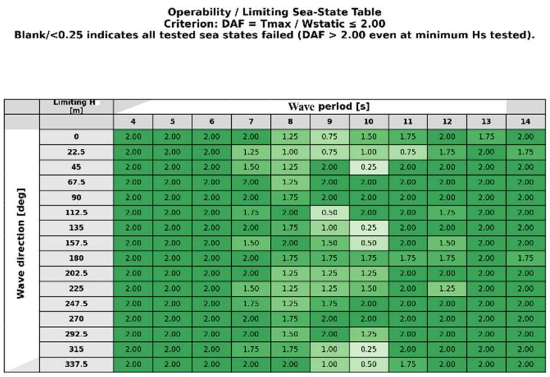

(a)

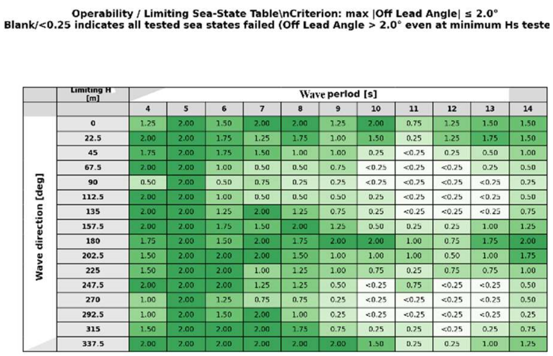

(b)

(c)

Figure 6- Operability plots for Lifting Off the Deck: (a) crane-cable dynamic amplification factor (DAF), with an acceptance limit of DAF ≤ 2.0; (b) absolute off-lead angle, with an acceptance limit of |off-lead| ≤ 2.0°; (c) absolute side-lead angle, with an acceptance limit of |side-lead| ≤ 2.0°.

5.3 Splash-zone response

The splash-zone operability results are presented in Figure 7. Figure 7(a) presents the crane-cable dynamic amplification factor (DAF), Figure 7(b) presents the absolute off-lead angle, and Figure 7(c) presents the absolute side-lead angle. The splash-zone phase is the governing stage of the operation.

Figure 7(a) shows that DAF is already restrictive at short periods. At $T = 4$–$5\ s$, the limiting sea state is commonly only about 0.25–0.75 m, and the DAF window broadens only gradually as the period increases. Figures 7(b) and 7(c) show that the lead-angle criteria impose additional restrictions across a broader intermediate-period band, especially around $T = 9$–$11\ s$, where many headings are limited to about 0.25–1.0 m and several cells approach failure at the minimum screened sea state. Off-lead and side-lead, therefore, remain critical even where the DAF window has partially recovered.

The key point is that the splash-zone phase governs not because it produces the largest DAF everywhere, but because it yields the narrowest combined operability envelope when all criteria are considered together. This behaviour is fully consistent with the adopted hydrodynamic model, in which sea-surface crossing activates both the additional axial added-mass term represented by the AxialAddedMassTopSeaSurface buoy and the entrapped-water inertia represented by the ExtraMassTrappedWater buoy. Accordingly, the splash-zone phase is governed by free-surface-entry hydrodynamics rather than by simple hook-load amplification. This is a defining characteristic of suction-caisson-type structures and is central to understanding why the SDU foundation suction caisson differs from more open-frame subsea structures.

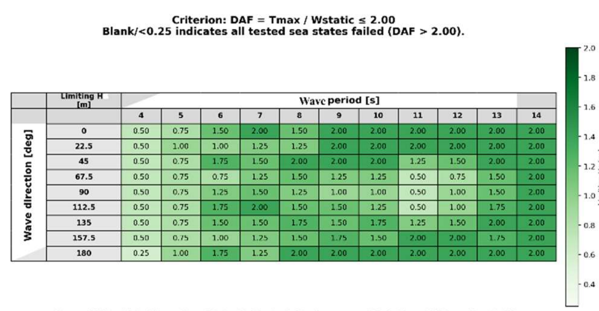

(a)

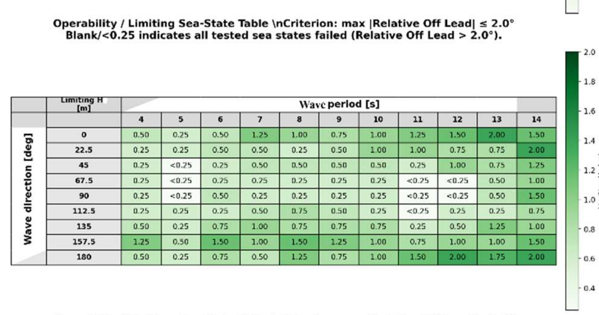

(b)

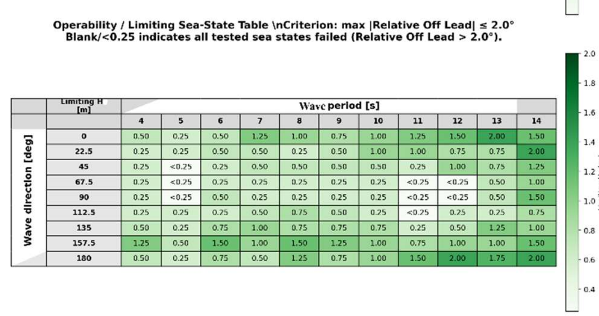

(c)

Figure 7- Operability plots for Splash Zone: (a) crane-cable dynamic amplification factor (DAF), with an acceptance limit of DAF ≤ 2.0; (b) absolute off-lead angle, with an acceptance limit of |off-lead| ≤ 2.0°; (c) absolute side-lead angle, with an acceptance limit of |side-lead| ≤ 2.0°.

5.4 Lowering below the splash zone

The operability results for the lowering stage are shown in Figure 8. Figure 8(a) presents the crane-cable dynamic amplification factor (DAF), Figure 8(b) presents the absolute off-lead angle, and Figure 8(c) presents the absolute side-lead angle. Once the SDU foundation is fully submerged, the response becomes more stable overall than in the splash zone.

Figure 8(a) shows that the DAF window broadens again after full submergence. For much of the investigated period range, especially from about 6 s upward, the limiting sea state is between about 1.5 and 2.0 m, and many cases reach the upper screened limit of 2.0 m. Figures 8(b) and 8(c) indicate that off-lead and side-lead still constrain selected combinations of period and heading, particularly around intermediate periods, but the most restrictive regions are less extensive than in the splash zone, and long-period conditions are generally more operable. The lowering response, therefore, remains angle-sensitive in some sectors, yet it does not define the governing weather window.

These results indicate that once the SDU foundation is fully submerged, the transient free-surface-crossing mechanisms become less important and hydrodynamic damping becomes more effective. The lowering phase is therefore more stable and more operable overall than the splash-zone phase.

Criterion: DAF = Tmax / Wstatic ≤ 2.00
Blank/<0.25 indicates all tested sea states failed (DAF > 2.00).

Wave direction [deg] \ Limiting H [m]	Wave period [s] 4	5	6	7	8	9	10	11	12	13	14
0	0.75	1.75	2.00	2.00	2.00	2.00	2.00	2.00	2.00	2.00	2.00
22.5	1.25	1.75	2.00	2.00	1.75	2.00	2.00	2.00	2.00	2.00	2.00
45	1.50	2.00	2.00	2.00	2.00	2.00	1.75	0.75	1.00	2.00	2.00
67.5	0.75	1.75	2.00	1.75	1.50	1.50	1.00	0.25	0.50	1.50	2.00
90	1.50	1.50	2.00	1.25	2.00	1.75	1.00	0.25	0.25	1.25	2.00
112.5	1.25	2.00	2.00	1.50	1.75	1.75	1.75	0.25	0.50	1.50	2.00
135	1.00	2.00	2.00	2.00	2.00	1.75	2.00	1.50	0.75	2.00	2.00
157.5	1.25	2.00	2.00	2.00	2.00	2.00	2.00	2.00	1.50	1.75	2.00
180	1.25	1.75	2.00	2.00	2.00	2.00	2.00	2.00	2.00	2.00	2.00

(a)

Operability / Limiting Sea-State Table \nCriterion: max |Off Lead Angle| ≤ 2.0°
Blank/<0.25 indicates all tested sea states failed (Off Lead Angle > 2.0°).

Wave direction [deg] \ Limiting H [m]	Wave period [s] 4	5	6	7	8	9	10	11	12	13	14
0	1.75	2.00	2.00	1.75	1.00	0.75	0.75	1.25	2.00	2.00	2.00
22.5	1.25	1.25	0.75	0.75	0.75	0.50	0.50	1.50	2.00	2.00	2.00
45	2.00	0.75	0.50	0.75	0.50	0.50	0.50	0.25	1.25	2.00	2.00
67.5	1.25	0.50	0.50	0.50	0.50	0.50	0.25	<0.25	0.50	1.25	2.00
90	1.50	0.50	0.75	0.50	0.50	0.25	0.25	<0.25	0.25	0.75	1.75
112.5	1.25	1.00	0.50	0.75	1.00	0.50	0.25	<0.25	0.50	1.00	1.50
135	1.25	1.50	1.00	2.00	0.75	1.00	0.25	0.75	0.75	2.00	1.75
157.5	1.25	1.50	2.00	2.00	2.00	1.25	0.75	0.75	2.00	1.75	2.00
180	1.50	1.25	2.00	1.75	2.00	1.00	1.00	1.25	2.00	2.00	2.00

(b)

Operability / Limiting Sea-State Table\nCriterion: max |Side Lead Angle| ≤ 2.0°
Blank/<0.25 indicates all tested sea states failed (Side Lead Angle > 2.0°).

Wave direction [deg] \ Limiting H [m]	Wave period [s] 4	5	6	7	8	9	10	11	12	13	14
0	1.75	1.50	0.50	1.00	0.50	0.25	0.50	1.25	2.00	2.00	2.00
22.5	1.25	2.00	1.00	0.75	0.50	0.75	0.75	1.50	2.00	2.00	2.00
45	2.00	1.25	1.75	2.00	2.00	1.00	0.75	0.25	1.25	2.00	2.00
67.5	1.50	1.50	2.00	1.50	0.50	1.00	0.25	<0.25	0.75	1.50	2.00
90	1.75	1.25	2.00	0.75	1.50	1.25	0.50	<0.25	0.25	1.25	2.00
112.5	1.25	1.00	1.75	1.25	0.50	0.25	0.25	<0.25	0.50	1.00	2.00
135	1.25	1.50	0.50	0.50	0.50	0.25	0.25	0.50	1.00	1.75	2.00
157.5	1.25	0.50	0.50	0.50	0.50	0.25	0.25	1.00	1.50	1.75	2.00
180	1.50	1.25	0.75	0.50	0.50	0.50	0.50	1.00	2.00	2.00	2.00

(c)

Figure 8- Operability plots for Lowering: (a) crane-cable dynamic amplification factor (DAF), with an acceptance limit of DAF ≤ 2.0; (b) absolute off-lead angle, with an acceptance limit of |off-lead| ≤ 2.0°; (c) absolute side-lead angle, with an acceptance limit of |side-lead| ≤ 2.0°.

5.5 Case study on the influence of axial added mass and entrapped-water modelling

To illustrate the effect of the auxiliary hydrodynamic buoys on the predicted lowering response, a dedicated case study was conducted under a single regular-wave condition with a wave direction of 0°, a significant wave height $H = 0.5$ m, and a peak period $T = 6$ s. The objective of this comparison was to isolate the influence of the two local hydrodynamic corrections introduced at sea-surface crossing, namely the entrapped-water buoy and the axial-added-mass buoy.

Three model variants were considered: (i) a base hollow-body model in which the lowering simulation was run without the two auxiliary buoys representing axial added mass and entrapped-water inertia; (ii) an entrapped-water model in which the lowering simulation was repeated with the ExtraMassTrappedWater buoy activated while the axial-added-mass buoy remained inactive; and (iii) a full sea-surface-crossing model in which the lowering simulation was run with both auxiliary buoys activated, namely ExtraMassTrappedWater and AxialAddedMassTopSeaSurface.

The comparison was based on crane-cable tension and crane-cable declination during the lowering stage. This case study was introduced to show how progressively refining the hydrodynamic idealisation affects the predicted response as the

SDU foundation passes through the free-surface and continues into the submerged-lowering stage. In this way, the relative contribution of entrapped-water inertia alone can be distinguished from the combined effect of entrapped-water inertia and the additional axial added mass that develops when the upper cap crosses the sea surface.

Figure 9 compares the crane-cable tension and crane-cable declination time histories for the three modelling cases. The base model without the two auxiliary buoys shows only a modest transient response when the structure crosses the free surface. The effective tension decreases smoothly from the pre-entry level and then settles at a lower post-entry level with comparatively limited oscillation. When the entrapped-water buoy is activated, a markedly stronger transient develops at about t = 1900 s, with a clear tension overshoot followed by a decaying oscillatory response. When both the entrapped-water buoy and the axial-added-mass buoy are activated, the transient becomes strongest, and the post-entry oscillations persist for the longest duration.

The difference is particularly clear in the tension histories. Over the interval 0–3000 s, the base model varies between approximately 572 and 680 kN. With only the entrapped-water buoy, the peak tension increases to about 779 kN, and the minimum drops to about 486 kN. With both auxiliary buoys activated, the peak rises further to about 907 kN, and the minimum decreases to about 419 kN. The declination histories remain close to 180° in all three cases, but the post-entry oscillations become denser and more persistent when the auxiliary buoy modelling is activated, especially in the full model with both buoy corrections. The case study, therefore, shows that the inclusion of entrapped-water inertia and axial added mass most strongly affects the lowering response through transient fluctuations in crane-cable tension associated with sea-surface crossing.

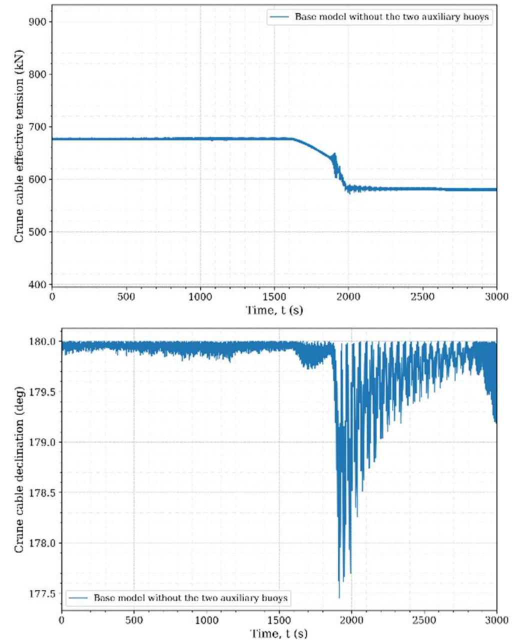

(a)

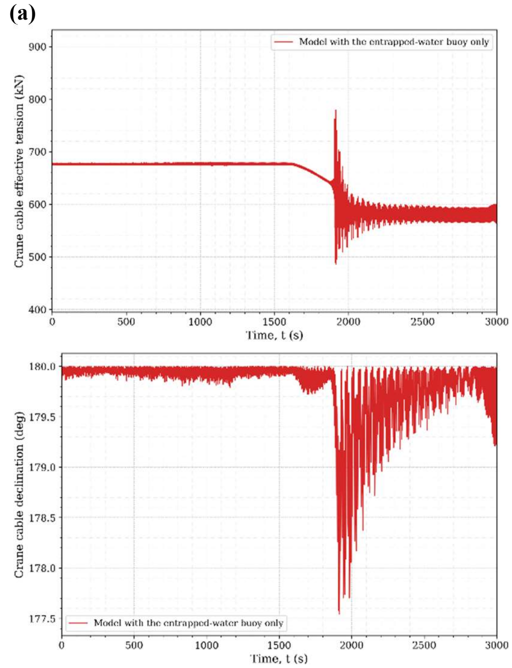

(b)

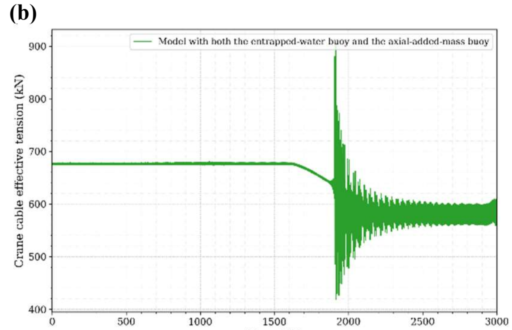

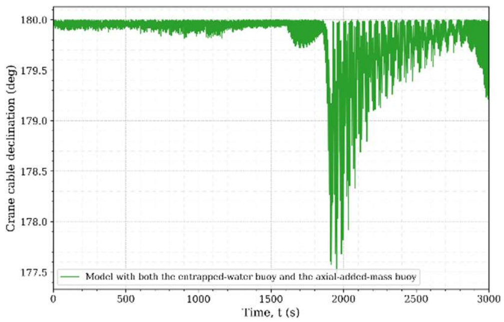

(c)

Figure 9- Case-study comparison of crane-cable response during lowering for wave direction 0°, *H* = 0.5 m, and *T* = 6 s, for (a) the base model without the two auxiliary buoys, (b) the model with the entrapped-water buoy only, and (c) the model with both the entrapped-water buoy and the axial-added-mass buoy. The figure includes both crane-cable tension and crane-cable declination time histories for the three modelling cases.

This case-study comparison provides a direct numerical demonstration of the modelling philosophy adopted in the present paper. The base hollow-body representation captures the global lowering behaviour of the SDU foundation, but it cannot fully reproduce the local hydrodynamic inertia effects associated with top-cap submergence. Adding the entrapped-water buoy introduces the inertia of the internal water column after submergence, whereas activating both auxiliary buoys provides the most complete representation of the free-surface-crossing physics used in the present study. The resulting increase in transient crane-cable tension and the longer decay of post-entry oscillations provide a practical measure of the importance of these modelling refinements in SDU foundation lowering analysis.

5.6 Comparative interpretation with PLET-type structures

The present SDU suction caisson foundation results are particularly instructive when compared with previously analysed open-frame subsea structures, such as Pipe Line End Terminal (PLET) foundations. In PLET-type structures, the governing installation stage may occur during lift-off from the barge, where the coupled vessel–wire–payload response in air produces the strongest restrictions. In the present SDU foundation case, however, the governing stage shifts to splash-zone entry.

This contrast shows that the governing installation stage is not universal but depends on structural topology and hydrodynamic mechanism. Open-frame structures are more strongly controlled by pre-submergence lifting dynamics, whereas suction-caisson-type structures may be governed by sea-surface crossing because the geometry activates additional axial added mass and entrapped-water inertia. Installation operability is therefore structure-dependent and cannot be generalised across subsea asset types.

6. Conclusions

A comprehensive time-domain OrcaFlex analysis was carried out to assess the operability of installing an SDU foundation lifted by a vessel from a cargo barge, lowered through the splash zone, and landed on the seabed at 154 m water depth. The study combined staged operational modelling, imported vessel-motion RAOs, and a hydrodynamic idealisation of the SDU foundation that explicitly represented the additional axial added mass and entrapped-water inertia associated with top-cap sea-surface crossing.

The results establish a clear hierarchy among the analysed installation stages. Lift-off is sensitive, but its DAF-based operability remains comparatively permissive; the main restrictions arise from off-lead and side-lead angles at selected headings and during intermediate periods. The splash-zone phase governs the overall operation and defines the narrowest operability envelope, as short-period cases are already limited by DAF, whereas a broader intermediate-period band is constrained by the angular response. After full submergence, the DAF window broadens again, and the lowering phase becomes more operable overall, although selected angle-governed combinations remain restrictive.

The case study confirms the physical importance of the auxiliary buoy modelling. Relative to the base model without the two auxiliary buoys, activating the entrapped-water buoy increases the peak crane-cable tension from about 680 kN to 779 kN, while activating both the entrapped-water buoy and the axial-added-mass buoy raises it to about 907 kN and produces the longest post-entry oscillations. The declination response remains close to 180° in all cases, but the persistence of the post-entry oscillations increases when the auxiliary hydrodynamic corrections are activated. The governing response is therefore controlled not simply by mean load level, but by the transient amplification generated when the caisson cap crosses the water surface.

The present study, therefore, shows that the governing installation stage is geometry-dependent. For the analysed SDU suction caisson foundation, splash-zone entry governs operability. This contrasts with more open-frame subsea structures, for which the most restrictive response may occur during pre-submergence lift-off. Accordingly, installation operability should not be generalised across structure types without accounting for the underlying hydrodynamic mechanism.

The developed methodology and resulting operability envelopes provide a practical basis for offshore planning, weather window definition, and phase-specific execution control for SDU foundation installation. The analysis also offers a useful framework for future comparative studies of subsea lifting operations involving different structural topologies and different governing hydrodynamic mechanisms.

7. References

1. de Andrade EM, Barral M, Cueva M, Fernandes AC. A review on the modeling of subsea lifting operations. Ocean Eng. 2023;271:113680.

2. Jia D, Agrawal M. Fluid-structure interaction: lowering subsea structure/equipment in splash zone during installation. In: Proceedings of the Offshore Technology Conference; 2014; Houston, TX. Houston (TX): Offshore Technology Conference; 2014.

3. Li Y, Zhao H, Xu N, et al. Study of the installation process of the subsea tree passed through the splash zone. Energies. 2020;13(5):1014.

4. Amer AM, Metrikine A, Gao Z. Dynamic analysis of splash-zone crossing operation for a subsea template. Sustain Mar Struct. 2022;4(2):19-40.

5. Gordon RB, Grytoyr G, Dhaigude M. Modeling suction pile lowering through the splash zone. In: Proceedings of the ASME 32nd International Conference on Ocean, Offshore and Arctic Engineering (OMAE2013); 2013; Nantes, France. New York (NY): ASME; 2013.

6. Yasseri SF, Bahai H. Availability assessment of subsea distribution systems at the architectural level. Ocean Eng. 2018;153:399-411.

7. Orcina Ltd. OrcaFlex. Version 11.6b [computer software]. Ulverston (UK): Orcina Ltd.

8. DNV-RP-C205: Environmental conditions and environmental loads. Recommended practice. Høvik (Norway): DNV.

9. DNV-RP-N103: Modelling and analysis of marine operations. Recommended practice. Høvik (Norway): DNV; 2017. Amended 2021.

10. Orcina Ltd. F07 suction anchor lowering. OrcaFlex example documentation. Ulverston (UK): Orcina Ltd. Available from Orcina example files/documentation.